Journal of the Nigerian Society of Physical Sciences

Synthesis and in vitro bioactivity of sodium metasilicate-derived silicon-substituted hydroxyapatite

Enobong R. Essien [ID]a,*, Violette N. Atasie[a], Ngozi A. Adeleye[a], Luqman A. Adams[b]

aDepartment of Chemical Sciences, Bells University of Technology, Ota 112103, Nigeria
bDeparment of Chemistry, University of Lagos, Akoka, Yaba100213, Nigeria

Abstract

Structural alteration of synthetic implants aims to achieve better bioactivity, higher cellular response, and regulated degradability, all of which are critical criteria for a biomaterial to serve as a graft in bone regeneration. The aim of this work was to synthesize silicon-substituted hydroxyapatite and test its bioactivity in simulated body fluid (SBF) by proving the use of sodium metasilicate ($Na_2SiO_3.9H_2O$) as an affordable precursor of silica. Thus, the study evaluated the *in vitro* bone-bonding capacity of hydroxyapatite ($Ca_{10}(PO_4)_6(OH)_2$) (HA) substituted with silicate ion ($Ca_{10}(PO_4)_{6-x}(SiO_4)_x(OH)_{2-x}$; Si_xHA). The Si_xHA with $x = 0.4$ was synthesized by utilizing a wet precipitation method with sodium metasilicate as a low-cost silica alternative for alkoxysilane precursors. The Si_xHA was then examined for properties such as morphology, elemental composition, phase composition, and the nature of chemical bonds using scanning electron microscopy (SEM), energy dispersive X-ray analysis (EDX), X-ray diffractometry (XRD), and Fourier transformed infrared spectroscopy (FTIR), respectively. An *in vitro* bioactivity experiment was also carried out by incubating the Si_xHA in simulated body fluid (SBF) at 36.5 °C for 7 and 14 days. The obtained results revealed the substitution of SiO_4^{4-} for some PO_4^{3-} groups in the hydroxyapatite structure. The Si_xHA nucleated more apatite crystals on its surface and demonstrated some degradability during the periods of immersion in SBF. The characteristics of the Si_xHA imply that it could be used as a graft in bone restoration applications, thus signifying that sodium metasilicate could serve as an economic silica source for silicon-substituted hydroxyapatite production.

Communicated by: Emmanuel Etim

1. Introduction

Hydroxyapatite (HA) ($Ca_{10}(PO_4)_6(OH)_2$) is the chemical compound that is present in the mineral phase of bone [1]. Because HA has a comparable chemical composition to the inorganic component of bone and is both biocompatible and osteoconductive, it is used as a graft material in reconstructive surgery [2]. The ability of the crystalline structure of HA to partially substitute calcium, orthophosphate, and hydroxyl ions is a highly interesting characteristic. Furthermore, biological apatite can undergo different substitution patterns, resulting in a variety of compositions. As a result, a carbonate hydroxyapatite that lacks calcium and hydroxyl (biological or bioapatite) contains a range of ions, including Na^+, K^+, Mg^{2+}, Zn^{2+}, HPO_4^{2-}, SiO_4^{4-}, Cl^-, and F^- [3–8].

Silicon incorporation into apatite has received special interest as a potential bone-replacement material. Carlisle's ground-
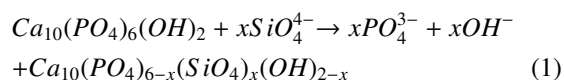
---

*Corresponding Author Tel. No.: +234-813-944-7446;

Email address: reggiessien@gmail.com; (Enobong R. Essien [ID])

breaking animal study according to Refs. [9–12], revealed that silicon plays an important role in bone tissue metabolism. Si deposition rose in young rodents where fresh bone tissue was actively mineralizing; however, as the bones aged, the amount of this element reduced. Furthermore, a link between silicon and calcium concentration was discovered. Carlisle's experiment further demonstrated the importance of silicon in the process of skeletal growth by feeding chicks with high- and low-silicon diets for a month [10]. Thus, when silicon (in the form of Na_2SiO_3) was added to meals, the animals gained weight and showed normal growth; but, when silicon intake was inadequate, the animals' skeletons formed improperly, with smaller size and impaired bone mineralization. Hence, it was demonstrated that silicon is a trace element essential for healthy skeletal growth, particularly during the early stages of bone formation.

Schwarz [13] also discovered that three mucopolysaccharides include bonded forms of silicon: heparan sulfate, chondroitin 4-sulfate, and hyaluronic acid. Furthermore, silicon has been shown to have physiological roles in bone tissue growth, such as slowing bone resorption, as well as improving mechanical strength and bone mineral density (BMD) [14, 15].

The ease of ion substitution in hydroxyapatite, particularly partial substitution of PO_4^{3-} with SiO_4^{4-} has made it a popular technique in biomaterial engineering since the 1990s [3, 4]. The mechanism described by Gibson [16] states that hydroxyl groups are released to form vacancies that balance the charge difference when orthosilicate ions (SiO_4^{4-}) replace phosphate ions (PO_4^{3-}) as seen in equation 1.

$$Ca_{10}(PO_4)_6(OH)_2 + xSiO_4^{4-} \rightarrow xPO_4^{3-} + xOH^-$$
$$+Ca_{10}(PO_4)_{6-x}(SiO_4)_x(OH)_{2-x} \qquad (1)$$

Based on this mechanism, the value of x must be in the range of $0 \leq x \leq 2$.

Silicon-substituted hydroxyapatite (SiHA) can be made via a number of methods, including the sol-gel approach [17–19], solid-state reactions [20], hydrothermal method [21, 22], and controlled crystallization (precipitation) processes [16–23]. Precipitation is one of the techniques that is most frequently employed to produce medical-grade HA and SiHA powders due to its benefits in terms of low temperature and reaction time, low cost, ease of use, small particle sizes, high purity, and comparatively good surface uniformity [24, 25]. In order to enhance the appeal and advantages of the wet precipitation method for industrial production, it would be excellent to replace alkoxysilane, the conventional silica precursor, with an affordable silica source. The goal of this work was to produce silicon-substituted hydroxyapatite and assess the bioactivity of the substance in SBF by demonstrating the usage of sodium metasilicate ($Na_2SiO_3.9H_2O$) as an inexpensive precursor of silica

2. Materials and methods

2.1. Materials

The materials acquired from Sigma-Aldrich (St. Louis, MO, USA) were utilized to synthesize HA and SiHA. The following were the reagents: ammonium hydroxide solution (NH_4OH), calcium nitrate tetrahydrate ($Ca(NO_3)_2.4H_2O$), sodium metasilicate ($Na_2SiO_3.9H_2O$) and disodium hydrogen phosphate dodecahydrate ($Na_2HPO_4.12H_2O$).

2.2. Synthesis of hydroxyapatite and silicon-substituted hydroxyapatite

To synthesize the HA, a novel approach was adopted whereby $Na_2HPO_4.12H_2O$ was used as the phosphate source instead of traditional diammonium hydrogen phosphate (($NH_4)_2HPO_4$). $Na_2HPO_4.12H_2O$ (9.10 g) was thoroughly dissolved in deionized water (200 mL). The solution was added gradually under constant stirring with a magnetic stirrer/heating device to a 334 mL solution containing ($Ca(NO_3)_2.4H_2O$) (10.0 g). The reaction temperature was maintained at 85 °C ($\pm$5 °C) while the pH of the mixture was kept at 9 ($\pm$0.25) by adding NH_4OH solution [26]. After the final addition, the reaction mixture was agitated for 15 min. The precipitate formed was centrifuged, washed with deionized water to remove residual Na ions and dried at 90 °C, then heated in a muffle furnace at 800 °C for 5 h for removal of nitrates and densification. This sample was named HA_w. The equation of the reaction is proposed in equation 2.

For the silicon-substituted HA synthesis, $Na_2HPO_4.12H_2O$ (8.48 g) and $Na_2SiO_3.9H_2O$ (0.49 g) were initially dissolved in 200 mL of deionized water. This was then mixed with 334 mL of $Ca(NO_3)_2.4H_2O$ (10.0 g) and the mixture was processed in a manner akin to that used in the manufacture of HA_w. Equation 3 shows the suggested reaction equation to form the silicon-substituted hydroxyapatite powder.

Based on the idea that one silicate ion would replace one phosphate ion, as shown in equation 1, the weights of the chemicals to be used were calculated. As a result, the ratio Ca/(P+Si) = 10/6 was kept constant. Table 1 lists the moles of each atom (Ca, P, and Si) in the initial aqueous solutions together with the anticipated silicon molar content per unit cell of apatite (x). The silicon-substituted hydroxyapatite was manufactured based on the value of x = 0.4, and referred to as Si_xHA.

2.3. Characterzation

With the aid of a scanning electron microscope, the samples' microstructures were evaluated (SEM: JEOL JSM 7660F; Tokyo, Japan). In order to enable visual monitoring of the samples under a 15 kV accelerating voltage, they were first affixed to a sample holder using carbon adhesives.

By obtaining the diffraction patterns from an X-ray diffractometer (XRD; Rigaku D/Max-IIIC, Tokyo, Japan) that used a CuKα radiation source with a wavelength of 0.154060 nm at 40 kV and 40 mA in the 2θ range from 10 to 70°, the mineral components and crystalline properties of the samples were ascertained. Before being examined, the samples were first reduced to a uniformly fine powder.

Fourier transform infrared spectroscopy (FTIR: Cary 630, Agilent Technologies; Santa Clara, CA, USA) was used on the samples in the wavenumber range of 4000–650 cm^{-1} in order to determine the chemical bond characteristics in the samples.
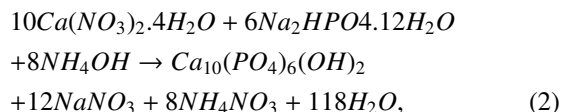
Table 1. Number of moles of atoms in the precursors and the anticipated Si content (x) in the samples

Sample	Ca(mol)	P (mol)	Si(mol)	x (mol)	Ca/P molar ratio
HA_w	0.64	0.384	0	0	1.667
Si_xHA	0.64	0.358	0.026	0.4	1.788

Attenuated Total Reflectance (ATR) was the mode of operation for the machine.

2.4. Bioactivity experiment in simulated body fluid (SBF)

By immersing the samples in SBF at physiological conditions (pH of 7.4 and temperature of 36.5 °C), according to a standard *in vitro* technique outlined by Kokubo and Takadama [27], the bioactivity of the samples was assessed. The following analytical grade reagents were used to make the SBF: tris(hydroxymethyl) aminomethane (Tris-buffer) $(CH_2OH)_3CNH_2)$, KCl, NaCl, $NaHCO_3$, $MgCl_2 \cdot 6H_2O$, $CaCl_2$, Na_2SO_4, and $K_2HPO_4 \cdot 3H_2O$ (Sigma-Aldrich, St. Louis, MO, USA). After the SBF was added to pristine screw-capped plastic bottles holding the samples, the bottles were put in an incubator and left for 7 or 14 days. 100 mL of SBF was used to soak 1g of each sample. Following the completion of each SBF incubation period, the sample was extracted from the supernatant using a vacuum pump filtering method. Enough deionized water was then added, and the mixture was gently spun before being left to dry for five days at 36.5 °C in an incubator.

$$10Ca(NO_3)_2.4H_2O + 6Na_2HPO4.12H_2O$$
$$+8NH_4OH \rightarrow Ca_{10}(PO_4)_6(OH)_2$$
$$+12NaNO_3 + 8NH_4NO_3 + 118H_2O, \quad (2)$$

3. Results and discussions

3.1. Microstructural properties

Figure 1 displays the images containing the microstructural features of the as-sintered samples. The surface of the HA_w micrograph (Figure 1a) showed HA beads with fragmented and clumped parts, resulting in asymmetrical forms. Due to the evenly distributed particles on the sample' surface, it was found that the surface appeared broad. Significant change was seen in the microstructure of Si_xHA (Figure 1b) following the replacement of some PO_4^{3-} with SiO_4^{4-} ions in the HA lattice. While a very small percentage of the particles continued to exist as beads and displayed a generally good particle distribution on the surface of the prepared glass sample, the majority of the particles took on a flaky morphology. The material now has a comparatively rougher surface as a result of this microstructure evolution. As the result shows, there has been a dramatic transformation of the surface chemistry through improvements in topography and physical qualities, resulting in a vast surface area with intrinsic surface roughness. The surface characteristics exhibited by Si_xHA are known to be associated with better protein and cell adhesion, which in turn promotes bone bonding through osteogenic differentiation and osteointegration of the material if used *in vivo* bone grafting [28].
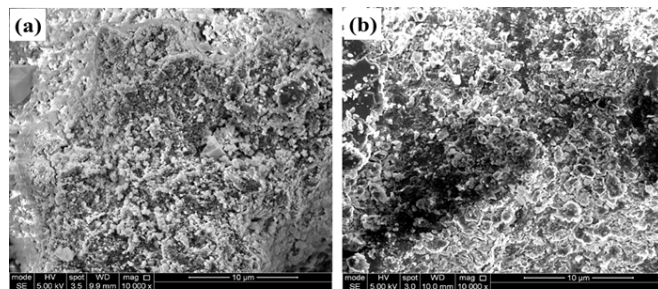

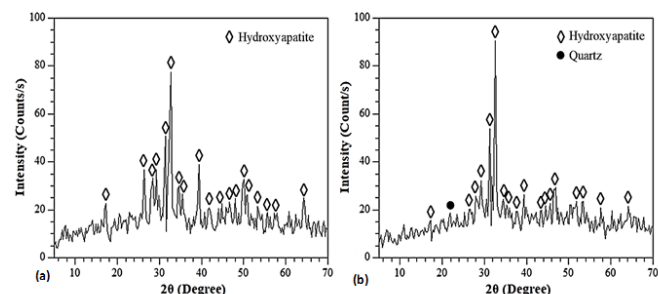Figure 1. SEM micrographs (a) HA_w (b) Si_xHA after sintering at 800 °C for 5 h.

Figure 2. Diffraction patterns showing the phase composition of (a) HA_w and (b) Si_xHA.

3.2. Phase and elemental composition

Figure 2 displays the diffraction patterns of the as-sintered HA_w and Si_xHA. The successful synthesis of HA in the sample was shown by the diffraction peaks of HA_w (Figure 2a), which matched the standard JCPDS file (card number 9-0432) [29]. Based on their intensity and baseline appearance, the peaks showed signs of semicrystalline glass-ceramic material. As shown in the spectrum, they have the following angular locations and corresponding crystal plane indices: 2θ 16.8° (101), 25.8° (002), 28° (102), 28.9° (210), 32.9° (300), 39.8° (310), 42° (131), 46.6° (222), 49.4° (213), and 65° (111).

When 0.4 mole of SiO_4^{4-} was added to replace PO_4^{3-}, there was a little increase in crystallinity (Figure 2(b)). Not to mention, at 2θ 22°, a little peak identified as quartz (SiO_2) appeared, confirming that SiO_4^{4-} added to the HA structure.

The elemental composition of HA_w and Si_xHA as shown by the EDX analysis results, which are shown in Figure 3, further indicated the successful synthesis of silicon-substituted hydroxyapatite. The elemental composition of HA_w (Figure 3a) revealed the presence of all of the elements found in HA ($Ca_{10}(PO_4)_6(OH)_2$) in their appropriate ratios. The emergence of a C peak in the spectrum is caused by the sample absorbing
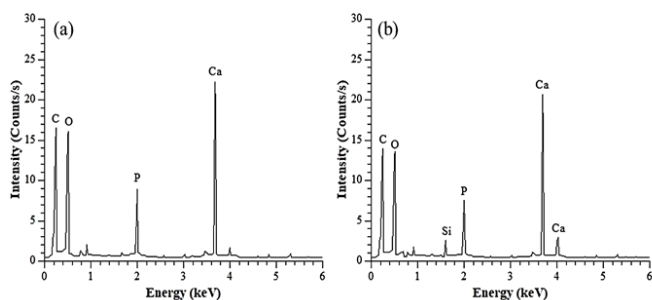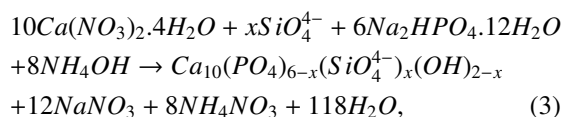
Figure 3. EDX spectra showing the elemental composition of (a) HA$_w$ and (b) Si$_x$HA.

Figure 4. FTIR spectra of (a) HA$_w$ and (b) Si$_x$HA before incubation in SBF showing the types of bonds present.

CO_2 during the synthesis process. The emergence of the Si peak in the spectrum of Si$_x$HA (Figure 3b) supports the production of silicon-substituted hydroxyapatite in the sample as indicated earlier in the XRD result of Si$_x$HA through the formation of quartz (SiO$_2$) phase (Figure 2b).

$$10Ca(NO_3)_2.4H_2O + xSiO_4^{4-} + 6Na_2HPO_4.12H_2O$$
$$+8NH_4OH \rightarrow Ca_{10}(PO_4)_{6-x}(SiO_4^{4-})_x(OH)_{2-x}$$
$$+12NaNO_3 + 8NH_4NO_3 + 118H_2O, \tag{3}$$

3.3. Chemical bonds

FTIR analysis was utilized to validate the nature of bonds found in the as-prepared samples. HA$_w$ (Figure 4a) exhibited strong peaks at 3362, 1640, 1088, and 1021 cm^{-1}. The broad band at 3362 cm^{-1} is attributed to the stretching vibration of OH in hydroxyapatite or water molecules absorbed by the sample, while the weak band near 1640 cm^{-1} represents the bending mode of surface water hydroxyl [30]. The sample's modest peak at 1088 cm^{-1} and the intense peak at 1021 cm^{-1} correspond to P-O asymmetric (v_3) stretching vibrations of the HPO$_4^{2-}$ and PO$_4^{3-}$ groups, respectively [31].

(Figure 4b) shows the FTIR spectrum of Si$_x$HA. As seen, additional peaks appeared in the spectrum after SiO$_4^{4-}$ replaced PO$_4^{3-}$ in the sample equation 3. The band appearing around 1474 cm^{-1} is attributed to the v_3 vibration of the CO$_3^{2-}$ group found in the B site of apatite, also known as carbonated apatite [31], which was earlier observed as a C peak in the EDX result (Figure 3). The PO$_4^{3-}$ group is responsible for the single P-O v_3 stretching vibration observed in the spectrum at 1021 cm^{-1}. Two new shoulder peaks appeared at 954 and 830 cm^{-1}, considered to be the stretching vibration Si-O bonds in SiO$_4^{4-}$ tetrahedrons located in apatite [32, 33] and the bending mode of CO$_3^{2-}$, respectively, and hence, confirming the successful incorporation of SiO$_4^{4-}$ to form silicon-substituted hydroxyapatite, as shown earlier in the XRD spectrum (Figure 2b) and EDX spectrum (Figure 3b). Thus, the absence of the P-O v_3 stretching vibrational mode for HPO$_4^{2-}$ could be ascribed to the SiO$_4^{4-}$ substitution for some PO$_4^{3-}$ in the HA structure resulting in low concentration of PO$_4^{3-}$ in the Si$_x$HA structure.

3.4. Bioactivity

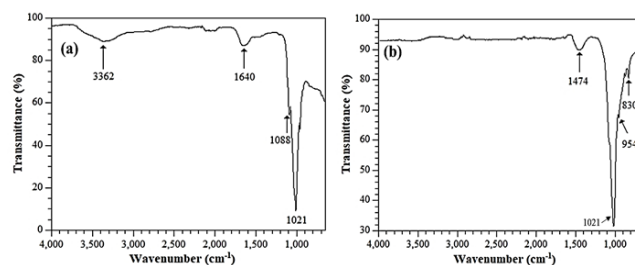The ability to undergo surface reactions to generate additional HA on the samples surfaces was examined after 7 and 14 days of incubating in SBF. To evaluate HA production, the samples were subjected to SEM, XRD, and FTIR spectroscopy analysis after being removed from SBF. (Figure 5a) shows the HA$_w$ microstructure after 7 days of incubating in SBF. Apatite crystals, which appear as thin flakes, dominate the sample's surface and are well distributed. After 14 days of immersion (Figure 5c), the surface became heterogeneous, with numerous microscopic HA crystallite balls embedded in larger flake-like particles. However, the microstructure of Si$_x$HA following incubation in SBF over the same time period was significantly different. After 7 days in SBF (Figure 5b), the sample surface was enriched with agglomerated balls of HA particles. These HA particles packed the sample's surface to the point that voids were rare when compared to HA$_w$ (Figure 5a). After 14 days of soaking, the HA on the sample's surface thickened, as seen from the positions of the microcracks (figure 5d). A silicate-based bioactive glass had previously demonstrated a similar shape [34]. HA production on a glass surface triggers a series of biological responses that culminate in bone mineralization on the synthetic scaffold [35].

Overall, the HA density on the surface of Si$_x$HA looked to be higher than that of HA$_w$, implying that Si$_x$HA was more bioactive than HA$_w$. This outcome is not entirely surprising, given that the surface morphological architecture of Si$_x$HA after sintering (Figure 1b) possessed better particle arrangement which gave rise to a high surface area and associated roughness. These properties enhanced the reactivity of the glass in SBF by promoting ion-exchange reaction on the glass surface resulting in higher bioactivity [36]. Figure 6 shows diffractograms that provide additional evidence of the materials' potential to produce HA nucleation after immersion in SBF. The diffractogram of HA$_w$ after 7 days of immersion in SBF (Figure 6a) shows a reduction in HA peak intensities. The HA peak reduction is also observed after 14 days of soaking HA$_w$ in SBF (Figure 6c). This pattern is maintained in Si$_x$HA after 7 and 14 days of incubation, as shown in (Figures 6b and 6d), respectively. Notably, at the same period of immersion in SBF, Si$_x$HA experienced a greater peak drop than HA$_w$ did. The reduction in HA peaks in the samples could be due to biodegradation. Bioactivity and biodegradability are two key characteristics for a bioactive glass used as a temporary graft in bone regeneration [37]. Si$_x$HA had a higher rate of biodegradability, thus corroborating the fact that it provided stronger ion-exchange interactions between the sample and SBF, resulting in increased bioactivity
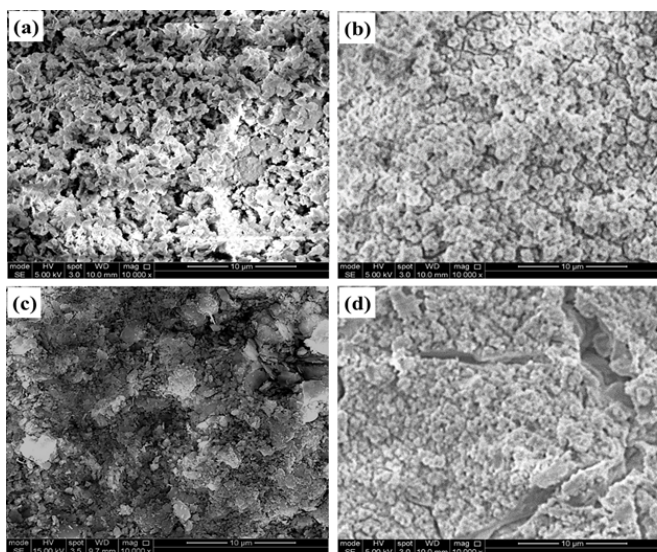
Figure 5. SEM micrographs of the samples after immersion in SBF; HA_w (a) 7 and (c) 14 days; Si_xHA (b) 7 and (d) 14 days.
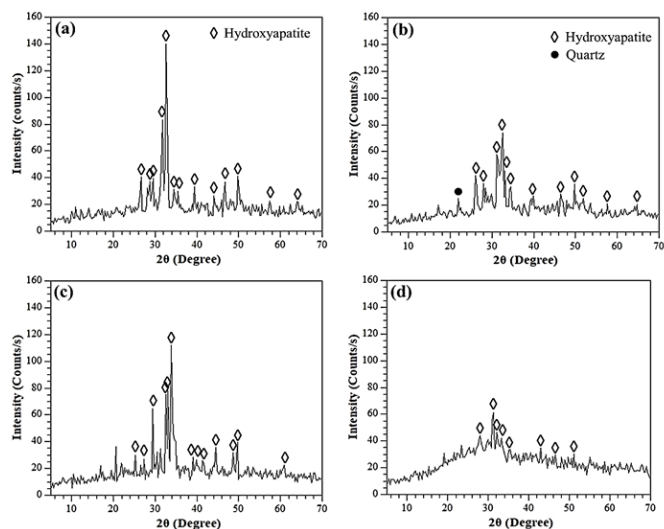

Figure 6. XRD spectra of the samples after immersion in SBF; HA_w (a) 7 and (c) 14 days; Si_xHA (b) 7 and (d) 14 days.

and degradation as suggested earlier. (Figure 7) depicts the chemical bond assessment of samples that were soaked for 7 and 14 days. The spectrum of HA_w after 7 days of immersion (Figure 7a) reveals a significant augmentation of the OH band at 3362 cm^{-1}, indicating greater HA deposition on the sample's surface. This is supported by an increase in the sharpness and intensity of the peak at 1640 cm^{-1}, which represents the bending mode of OH [29]. Furthermore, it is important to note that the asymmetric vibrational frequencies of P-O in HPO_4^{2-} and PO_4^{3-} groups, which are 1088 and 1021 cm^{-1}, respectively, remain unchanged. This could be attributed to the lack of structural variation after immersing in SBF for 7 days. However, after 14 days of immersion in SBF, a minor peak considered to
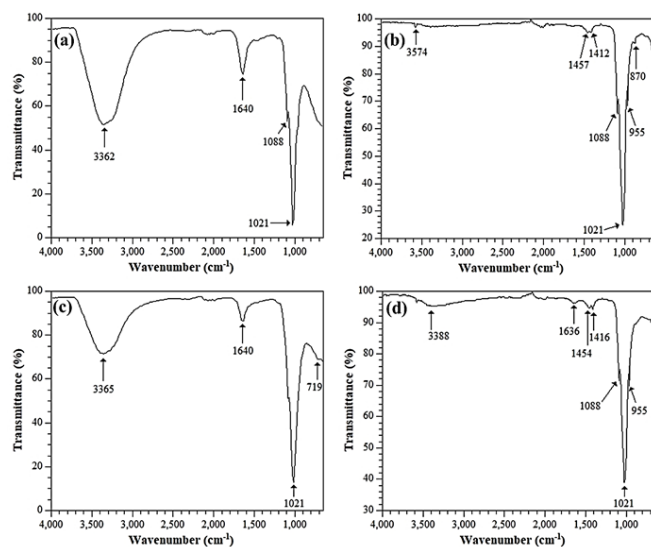

Figure 7. FTIR spectra of the samples after immersion in SBF; HA_w (a) 7 and (c) 14 days; Si_xHA (b) 7 and (d) 14 days.

be the asymmetric P-O bending of PO_4^{3-} [38] in HA appeared as a shoulder approximately at 719 cm^{-1} due to enhanced HA deposition caused by phosphate uptake from the SBF.

(Figure 7b) shows the vibrational mode of the bonds in Si_xHA after 7 days of immersing in SBF. There is a minor peak near 3574 cm^{-1} that corresponds to the OH stretching vibration of HA. The carbonate band, which was initially positioned at 1474 cm^{-1}, divided into two modes at 1457 and 1412 cm^{-1}, which are asymmetric stretching (v_3) doublets caused by CO_3^{2-} incorporation into the produced apatite layer, yielding carbonate hydroxyapatite (HCA) [39]. A minor peak at about 870 cm^{-1} indicates out-of-plane bending (v_2) of CO_3^{2-}, often associated with carbonate incorporation into the apatite layer [39]. This supports this notion.

The replacement of CO_3^{2-} for OH in the apatite structure could explain the low intense nature of the OH stretching vibrational peak and the lack of a peak for its bending mode. The development of a new phosphate peak at 1088 cm^{-1}, in addition to the existing one at 1021 cm^{-1}, suggests that the sample contains more apatite layers, while the bond associated with SiO_4^{4-} substitution is observed at 955 cm^{-1}. After 14 days of immersing the sample in SBF (Figure 7d), the OH band broadened at 3388 cm^{-1} due to hydrogen bonding caused by surface water absorption and the incorporation of more HA into the sample, as evidenced by the emergence of a water hydroxyl bending mode at 1636 cm^{-1}. The twin CO_3^{2-} peaks became significantly more pronounced, shifting to 1454 and 1416 cm^{-1}, whereas the phosphate and silicate vibrational peak frequencies remained constant.

These manifestations confirm the formation of additional HA on the surface of the samples during the periods of incubation in SBF as described earlier using the SEM and XRD results. Additionally, the FTIR results validated the superior ability of the silicon-substituted hydroxyapatite (Si_xHA) to nucleate more HA on its surface than the unsubstituted HA (HA_w)

when immersed in SBF for a similar duration.

4. Conclusions

A hydroxyapatite substituted with silicate ion ($Ca_{10}(PO_4)_{6-x}(SiO_4)_x(OH)_{2-x}$) was successfully produced with $x = 0.4$ by employing sodium metasilicate as the silicate source. Analysis with SEM, EDX, XRD, and FTIR verified the production of silicon-substituted hydroxyapatite. The *in vitro* bioactivity test, which involved immersing the pristine hydroxyapatite and silicon-substituted hydroxyapatite in SBF for 7-14 days, demonstrated that the latter had a greater capability for nucleating hydroxyapatite on its surface. Furthermore, the silicon-substituted hydroxyapatite demonstrated biodegradable characteristics after its immersion in SBF. These characteristics of are critical for a material to function as a graft in bone regeneration. Importantly, the synthetic technique used in this work, which used sodium metasilicate as the silica source instead of alkoxysilane, offers a significant advantage as a low-cost replacement, which could allow the process to be scaled up for commercial production.

Acknowledgment

References

[1] S. Daane, "Alloplastic implantation", in *Plastic Surgery Secrets Plus*, J. Weinzweig (Ed.), Mosby, St. Louis, United States, 2010, pp. 28–32. https://doi.org/10.1016/B978-0-323-03470-8.00005-3.

[2] H. A. Siddiqui, K. L. Pickering, & M. R. Mucalo, "A Review on the use of hydroxyapatite-carbonaceous structure composites in bone replacement materials for strengthening purposes", Materials (Basel) **11** (2018) 1813. https://doi.org/10.3390/ma11101813.

[3] A. Camaioni, I. Cacciotti, L. Campagnolo, & A. Bianco, "Silicon-substituted hydroxyapatite for biomedical applications", in *Hydroxyapatite (HAp) for Biomedical Applications*, M. Mucalo (Ed.), Woodhead Publishing, Cambridge, England, 2015, pp. 343–373. https://doi.org/10.1016/B978-1-78242-033-0.00015-8.

[4] J. H. Shepherd, D.V. Shepherd, & S. M. Best, "Substituted hydroxyapatites for bone repair", Journal of Materials Science: Materials in Medicine **23** (2012) 2335. https://doi.org/10.1007/s10856-012-4598-2.

[5] M. Vallet-Regí, & J. M. González-Calbet, "Progress in Solid State Chemistry", **32** (2004) 1. https://doi.org/10.1016/j.progsolidstchem.2004.07.001.

[6] R. Z. LeGeros, "Properties of osteoconductive biomaterials: Calcium phosphates", Clinical Orthopaedics and Related Research **395** (2002) 81. https://doi.org/10.1097/00003086-200202000-00009.

[7] S. V. Dorozhkin, & M. Epple, "Biological and medical significance of calcium phosphates", Angewandte Chemie International Edition **41** (2002) 3130. https://doi.org/10.1002/1521-3773(20020902)41:17⟨3130::AID-ANIE3130⟩3.0.CO;2-1

[8] S. V. Dorozhkin, "Bioceramics based on calcium orthophosphates. (Review)", Glass Ceramics **64** (2007) 442. https://doi.org/10.1007/s10717-007-0109-1.

[9] E. M. Carlisle, "Silicon: A possible factor in bone calcification", Science **167** (1970) 279. https://doi.org/10.1126/science.167.3916.279.

[10] E. M. Carlisle, "Silicon: an essential element for the chick", Science **178** (1972) 619. https://doi.org/10.1126/science.178.4061.619.

[11] E. M. Carlisle, "Silicon: a requirement in bone formation independent of vitamin D_1", Calcified Tissue International **33** (1981) 27. https://doi.org/10.1007/BF02409409.

[12] E. M. Carlisle, "Silicon as an essential trace element in animal nutrition", Ciba Foundation Symposium **121** (1986) 123. https://doi.org/10.1002/9780470513323.ch8.

[13] K. Schwarz, "A bound form of silicon in glycosaminoglycans and polyuronides", Proceedings of the National Academy of Sciences, USA **70** (1973) 1608. https://doi.org/10.1073/pnas.70.5.1608.

[14] M. Calomme, P. Geusens, N. Demeester, G. J. Behets, P. D'Haese, J. B. Sindambiwe, V. Van Hoof, & D. Vanden Berghe, "Partial prevention of long-term femoral bone loss in aged ovariectomized rats supplemented with choline-stabilized orthosilicic acid", Calcified Tissue International **78** (2006) 227. https://doi.org/10.1007/s00223-005-0288-0.

[15] B. D. Nielsen, G. D. Potter, E. L. Morris, T. W. Odom, D. M. Senor, J. A. Reynolds, W. B. Smith, M. T. Martin, & E. H. Bird, "Training distance to failure in young racing quarter horses fed sodium zeolite", Journal of Equine Veterinary Science **13** (1993) 562. https://doi.org/10.1016/S0737-08060681526-1.

[16] I. R. Gibson, S. M. Best, & W. Bonfield, "Chemical characterization of silicon-substituted hydroxyapatite", Journal of Biomedical Materials Research **44** (1999) 422. https://doi.org/10.1002/(sici)1097-4636(19990315)44:4⟨422::aid-jbm8⟩3.0.co;2-#

[17] A. J. Ruys "Silicon-doped hydroxyapatite", Journal of the Australian Ceramic Society **29** (1993) 71. https://www.docketalarm.com/cases/PTAB/IPR2013-00582/Inter_Partes_Review_of_U.S._Reissue_Pat._RE041251/09-12-2013-Petitioner/Exhibit-1014-AJ_Ruys,_Silicon_Doped_Hydroxyapatite/.

[18] A. A. Faremi, S. S. Oluyamo, K. D. Adedayo, Y. A. Odusote, & O. I. Olusola, "Influence of silicon nanoparticle on the electrical properties of heterostructured CdTe/CdS thin films based photovoltaic device", Journal of the Nigerian Society of Physical Sciences **3** (2021) 256. https://doi.org/10.46481/jnsps.2021.267.

[19] K. M. Omatola, A. D. Onojah, A. N. Amah, & I. Ahemen, "Synthesis and characterization of silica xerogel and aerogel fromrice husk ash and pulverized beach sand via sol-gel route", Journal of the Nigerian Society of Physical Sciences **5** (2023) 1609. https://doi.org/10.46481/jnsps.2023.5.1609.

[20] D. Arcos, J. Rodriguez-Carvajal, & M. Vallet-Regi, "The effect of the silicon incorporation on the hydroxylapatite structure. a neutron diffraction study", State Sciences **6** (2004) 987. https://doi.org/10.1016/j.solidstatesciences.2004.05.001.

[21] Y. Tanizawa, & T. Suzuki, "X-ray photoelectron spectroscopy study of silicate-containing apatite, Phosphorus", Phosphorus Research Bulletin **4** (1994) 83. https://doi.org/10.3363/prb1992.4.0_83.

[22] X.L. Tang, X.F. Xiao, & R.F. Liu, "Structural characterization of silicon-substituted hydroxyapatite synthesized by a hydrothermal method", Materials Letters **59** (2005) 3841. https://doi.org/10.1016/j.matlet.2005.06.060.

[23] D. Arcos, J. Rodriguez-Carvajal, & M. Vallet-Regi, "Silicon incorporation in hydroxylapatite obtained by controlled crystallization", Chemistry of Materials **16** (2004) 2300. https://doi.org/10.1021/cm035337p.

[24] G. Ma "Three common preparation methods of hydroxyapatite", IOP Conference Series Materials Science and Engineering **688** (2019) 033057. https://doi.org/10.1088/1757-899X/688/3/033057.

[25] M. Głab, S. Kudłacik-Kramarczyk, A. Drabczyk, J. Walter, A. Kordyka, M. Godzierz, R. Bogucki, B. Tyliszczak, & A. Sobczak-Kupiec, "Hydroxyapatite obtained via the wet precipitation method and PVP/PVA matrix as components of polymer-ceramic composites for biomedical applications", Molecules **26** (2021) 4268. https://doi.org/10.3390/molecules26144268.

[26] M. Palard, E. Champion, & S. Foucaud, "Synthesis of silicated hydroxyapatite $Ca_{10}(PO_4)_{6-x}(SiO_4)_x(OH)_{2-x}$", Journal of Solid State Chemistry **181** (2008) 1950. https://doi.org/10.1016/j.jssc.2008.04.027.

[27] T. Kokubo, & H. Takadama, "How useful is SBF in predicting in vivo bone bioactivity?", Biomaterials **27** (2006) 2907. https://doi.org/10.1016/j.biomaterials.2006.01.017.

[28] L. Lin, H. Wang, M. Ni, Y. Rui, T.-Y. Cheng, C.-K. Cheng, X. Pan, G. Li, & C. Lin, "Enhanced osteointegration of medical titanium implant with surface modifications in micro/nanoscale structures", Journal of Orthopaedic Transaction **2** (2014) 35. https://doi.org/10.1016/j.jot.2013.08.

001.

[29] S. Rahman, K. H. Maria, M. S. Ishtiaque, A. Nahar, H. Das, & S. M. Hoque, "Evaluation of a novel nanocrystalline hydroxyapatite powder and a solid hydroxyapatite/Chitosan-Gelatin bioceramic for scaffold preparation used as a bone substitute material", Turkish Journal of Chemistry **44** (2020) 884. https://doi.org/10.3906/kim-1912-40.

[30] N. Kourkoumelis, & M. Tzaphlidou, "Spectroscopic assessment of normal cortical bone: Differences in relation to bone site and sex", The Scientific World Journal **10** (2010) 402. https://doi.org/10.1100/tsw.2010.43.

[31] J.P. Lafon, E. Champion, & D. Bernache-Assollant, "Processing of AB-type carbonated hydroxyapatite $Ca_{10-x}(PO_4)_{6-x}(CO_3)_x(OH)_{2-x-2y}(CO_3)_y$ ceramics with controlled composition", Journal of the European Ceramic Society **28** (2008) 139. https://doi.org/10.1016/j.jeurceramsoc.2007.06.009.

[32] L. Boyer, J. Carpena, J. L. Lacout, "Synthesis of phosphate-silicate apatites at atmospheric pressure", Solid State Ionics **95** (1997) 121. https://doi.org/10.1016/S0167-27389600571-1.

[33] I. R. Gibson, S. M. Best, & W. Bonfield, "Chemical characterization of silicon-substituted hydroxyapatite", Journal of Biomedical Materials Research **44** (1999) 422. https://doi.org/10.1002/(sici)1097-4636(19990315)44:4⟨422::aid-jbm8⟩3.0.co;2-#.

[34] L. A. Adams, & E. R. Essien, "In Vitro Transformation of Sol-gel Derived Bioactive Glass from Sand", American Journal of Biomedical Sciences **7** (2015) 218. https://doi.org/doi:10.5099/aj150400218.

[35] T. Michigami, "Skeletal mineralization: mechanisms and diseases", Annals of Pediatric Endocrinology and Metabolism **24** (2019) 213. https://doi.org/10.6065/apem.2019.24.4.213.

[36] L. A. Adams, & E. R. Essien, "Bioactivity of Quaternary Glass Prepared from Bentonite Clay", Journal of Advanced Ceramics **5** (2016) 47. https://doi.org/10.1007/s40145-015-0172-y.

[37] N. G. Panah, R. Atkin, & T. B. Sercombe, "Bioactivity and biodegradability of high temperature sintered 58S ceramics", Journal of the European Ceramic Society **42** (2022) 3614. https://doi.org/10.1016/j.jeurceramsoc.2022.02.051.

[38] S. M. Smith, W. Maneeprakorn, & P. Winotai, "Phase and thermal stability of nanocrystalline hydroxyapatite prepared via microwave heating", Thermochimica Acta **447** (2006) 115. https://doi.org/10.1016/j.tca.2006.04.013.

[39] O. F. Yasar, W.-C. Liao, R. Mathew, Y. Yu, B. Stevensson, Y. Liu, Z. Shen, & M. Edén. "The carbonate and sodium environments in precipitated and biomimetic calcium hydroxy-carbonate apatite contrasted with bone mineral: structural insights from solid-state NMR", The Journal of Physical Chemistry C **125** (2021) 10572. https://doi.org/10.1021/acs.jpcc.0c11389.